

Continuous “Snowing” Thermo-therapeutic Graphene

Yangyong Sun, Zengzhen Chen, Huiping Gong, Xueqiao Li, Zhenfei Gao, Shichen Xu, Xiaodong Han, Bing Han,* Xianwei Meng,* and Jin Zhang*

Finding the best applications of graphene, and the continuous and scalable preparation of graphene with high quality and high purity, are still two major challenges. Herein, a “pulse-etched” microwave-induced “snowing” (PEMIS) process is developed for continuous and scalable preparation of high-quality and high-purity graphene directly in the gas phase, which is found to have excellent thermo-therapeutic effects. The obtained graphene exhibits small size (≈ 180 nm), high quality, low oxygen content, and high purity, together with a high gas–solid conversion efficiency of $\approx 10.46\%$. Considering the intrinsic characteristics of this high-purity and small-sized biocompatible graphene, in particular the low-frequency microwave absorption property as well as the good thermal transformation ability, a graphene-based combination therapeutic system is demonstrated for microwave thermal therapy (MTT) for the first time, exhibiting a high tumor ablation rate of $\approx 86.7\%$. This is different from the principle of ions vibrating in a confined space used by current MTT sensitization materials. Not limited to this application, it is foreseen that this PEMIS-based high-quality graphene will allow the search for further suitable applications of graphene.

Graphene has unrivalled mechanical, thermal, and electrical properties, but how to benefit from these properties and looking for the best applications of graphene have always been major concerns.^[1–5] Preparation makes the future. If we want to find the best applications of graphene, the first and foremost is to achieve the scalable preparation of high-quality graphene with high purity.^[6–9] Until now, finding the best applications of graphene, and the continuous and scalable preparation of graphene with high quality and high purity, have still been two major challenges.

One is how to realize the continuous and scalable preparation of graphene with high quality and high purity. Commercial scalable production of graphene mainly relies on traditional liquid-phase exfoliation methods, performed in a solvent and many defects or surface contaminations may be caused in graphene powder, losing

the fascinating properties of pristine graphene.^[8,10] Apart from this, the substrate-catalyzed chemical vapor deposition method can realize continuous production of high-quality graphene films in a roll-to-roll manner, but generally speaking, the process is complicated, and transfer has always been one of the bottlenecks for the applications of graphene films.^[11] How to get rid of the limitations of solvents or substrate and directly scalable preparation of high-quality as well as high-purity graphene still ongoing. Nowadays, the method for growing graphene in the gas phase has arisen at the historic moment, and it is usually realized by gas discharge without the assistance of catalysts or substrate but deriving a high-quality graphene.^[12–14] Internally excited arc discharge is a common form, but always accompanied by interference from by-products such as carbon tubes or graphite synthesized at high temperatures, affecting the purity.^[12] Exogenous excitation such as microwave^[13] or RF-induced^[15] gas phase discharge can effectively improve the purity of graphene prepared in the gas phase. However, the fact that the weakened or shielded excitation caused by prolonged graphene will bring about the degradation of graphene's quality has been an important factor that has been ignored,^[14] that is, continuous and scalable production of high-quality graphene cannot be achieved. Therefore, continuous production of high-quality and high-purity graphene should still be paid more attention.

Besides, developing specific application exports derived from the intrinsic characteristics of graphene is equally important.^[7,16] Taking advantage of the large specific surface area


Y. Sun, Dr. Z. Gao, S. Xu, Prof. J. Zhang
Center for Nanochemistry
Beijing Science and Engineering Center for Nanocarbons
Beijing National Laboratory for Molecular Sciences
College of Chemistry and Molecular Engineering
Peking University
Beijing 100871, China
E-mail: jinzhang@pku.edu.cn

Y. Sun, H. Gong, Dr. Z. Gao, S. Xu, Prof. J. Zhang
Beijing Graphene Institute
Beijing 100095, China

Z. Chen, Prof. X. Meng
Laboratory of Controllable Preparation and Application of Nanomaterials
Key Laboratory of Cryogenics
Technical Institute of Physics and Chemistry
Chinese Academy of Sciences
Number 29 East Road Zhongguancun, Beijing 100190, China
E-mail: mengxw@mail.ipc.ac.cn

X. Li, Prof. X. Han
Institute of Microstructure and Property of Advanced Materials
Beijing Key Lab of Microstructure and Property of Advanced Materials
Beijing University of Technology
Beijing 100124, China

Prof. B. Han
Department of Orthodontics
Peking University School and Hospital of Stomatology
Beijing 100081, China
E-mail: kqbinghan@bjmu.edu.cn

 The ORCID identification number(s) for the author(s) of this article can be found under <https://doi.org/10.1002/adma.202002024>.

DOI: 10.1002/adma.202002024

(SSA), high conductivity, and high thermal conductivity of graphene, fields such as sensing^[17] and drug loading,^[18] batteries and supercapacitors,^[19] as well as heat dissipation and heat conduction^[20] can be developed, respectively. Exploring suitable applications driven by the intrinsic properties of high-quality and high-purity graphene is still an urgent issue.

Herein, we have developed a continuous and scalable method for synthesizing high-quality and high-purity graphene powder, which was found to have excellent thermostherapeutic effects. This was achieved by a “pulse-etching” technology assisted microwave-induced “snowing” process. High-quality and high-purity “pulse-etch microwaved graphene” (PEMG) can be directly obtained in the gas phase without substrate or catalyst. Typically, a high yield of $\approx 10.46\%$ with I_D/I_G as low as ≈ 0.27 and I_{2D}/I_G as high as ≈ 1.06 can be realized. The PEMG exhibited a small size of ≈ 180 nm and an extremely high element ratio of C/O of ≈ 165 . No impurities of PEMG can be detected based on thermogravimetric. Based on the intrinsic characteristics of this high-purity and small-sized biocompatible graphene, especially low-frequency microwave absorption property as well as good thermal transformation ability, graphene-based combination therapeutic system was demonstrated for MTT for the first time, showing a high tumor ablation rate of $\approx 86.7\%$. This was different from the principle of ions vibrating in a confined space used by current MTT sensitization materials.^[21,22] This scalable graphene helps to expand the graphene family and is conducive to exploring the possibilities of graphene’s suitable applications.

The experiment was performed in an atmospheric pressure microwave (2.45 GHz) reaction chamber (Figure S1, Supporting Information). Similar to our previous work,^[14] PEMG was grown directly in the gas phase, that is, “snowing,” without any catalyst or substrate when introducing carbon sources such as methane in the Ar plasma. As the reaction continues, the inner wall of the quartz tube in the reactor is gradually surrounded by partially generated graphene, which not only acts as a “microwave absorption medium,” causing the input microwave to be absorbed by the graphene to generate heat, but also

serves as an “electromagnetic shielding layer,” affecting the continuous generation of plasma for continuous “snowing” graphene. To solve this problem, we have innovatively developed the “pulse-etching” technology to achieve continuous “snowing” graphene (Figure 1a). The introduction of the carbon sources and the etchant is performed alternately in a pulsed manner. After growing graphene for a period of time, the reaction gas is switched to the etchant (the choice of the etchant can be selected from oxygen, water vapor, carbon dioxide, etc.). The internal wrapped graphene absorbs heat for reaction in the presence of O₂ plasma (graphene + O₂ → CO₂), making the graphene etched clean in place (Figure S2, Supporting Information), while the resulting PEMG is not affected because it grows in the gas phase and drifts away from the system with the carrier gas. Therefore, continuous “snowing” graphene in a “growth-etch-growth-etch” manner can be achieved by the simplest replacement of the reaction gas atmosphere, which is conducive to large-scale production of graphene at low cost. Based on this technology, a large amount of PEMG can be obtained (Figure 1b), and the yield of PEMG can be as high as 10.46% (the g/g weight ratio of graphene/carbon sources) with a high quality, which is superior to that reported in other literatures (Figure 1c).^[13,14,23–25]

The obtained PEMG exhibits the characteristic of small size with an average size of ≈ 180 nm (Figure 2a). We found that the SSA of the obtained PEMG increases with decreasing methane concentration, and can reach 323 m² g⁻¹ at a low methane concentration of 0.083% (Figure 2b and Figure S3, Supporting Information), much superior to others (Table S1, Supporting Information). Electron energy loss spectroscopy (EELS) spectra of carbon K-edge region were conducted to investigate the structure of the synthesized PEMG. The peaks at about 284.6 and 291.8 eV can be corresponded to the 1s– π^* and 1s– σ^* transitions,^[13] respectively, and further confirm the sp² hybrid structure of PEMG (Figure 2c). Low-resolution transmission electron microscopy (TEM) indicates the few-layers characteristic of PEMG (Figure 2d,e and Figure S4, Supporting Information). High-resolution TEM shows that the layer spacing of

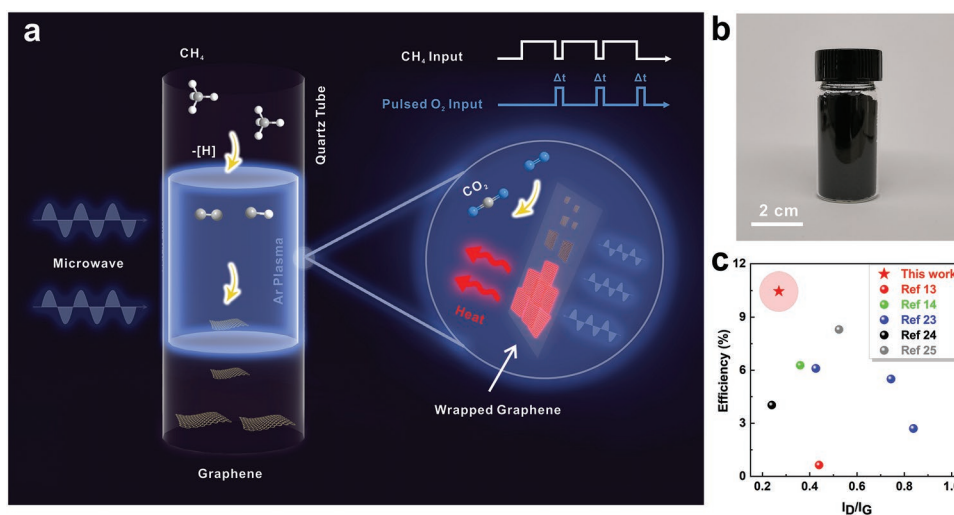


Figure 1. Schematic illustration of PEMIS and basic characterizations of PEMG. a) Scheme of PEMIS process. b) Photograph of PEMG powder. c) Comparison of the efficiency and I_D/I_G of graphene obtained in this work with others.^[13,14,23–25]

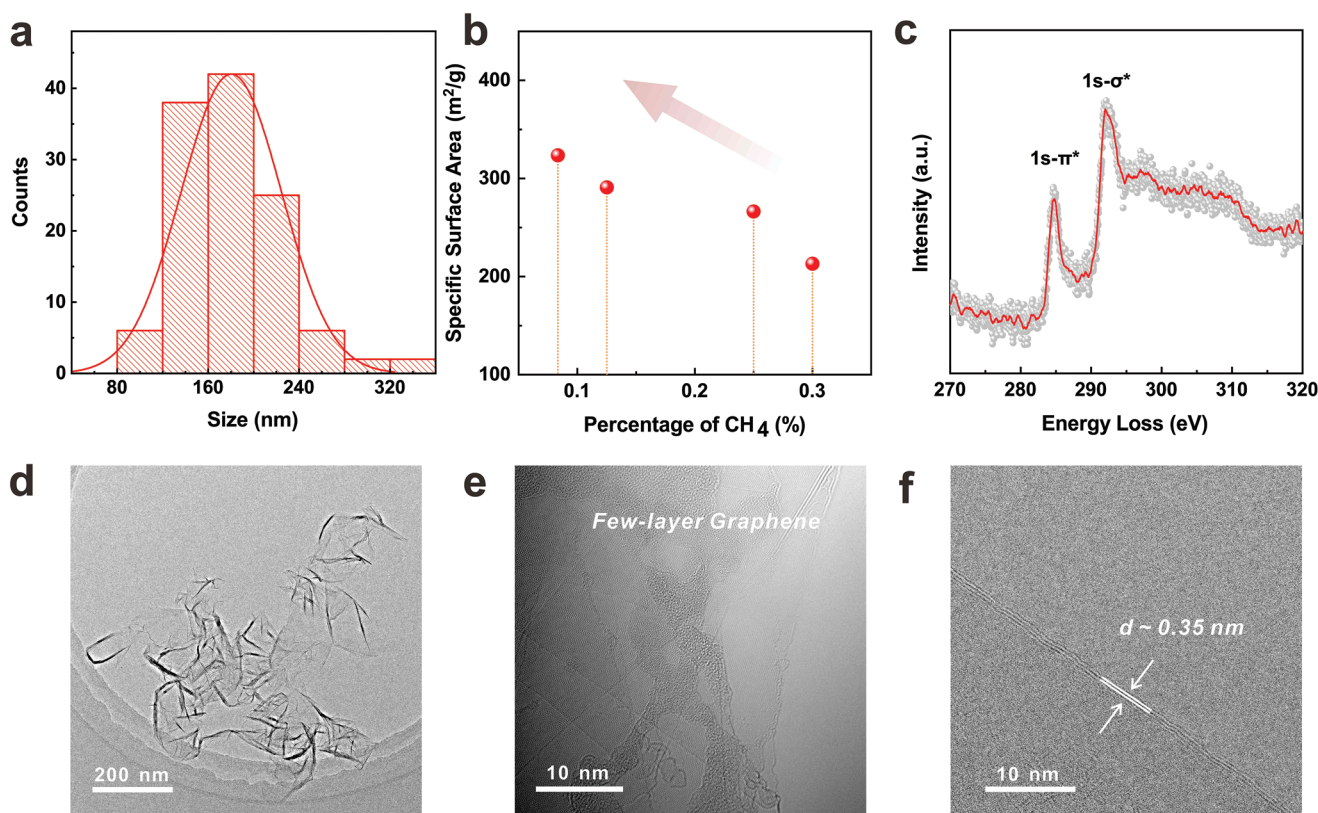


Figure 2. Characterizations and analysis of high-quality PEMG. a) Size distribution of PEMG at a methane concentration of 0.25%. b) Trend of SSA of PEMG over methane concentrations. c) EELS spectra of PEMG, showing sp² hybrid structure. d) Low-magnification TEM image of PEMG. e, f) High-resolution TEM image of the edges of PEMG; a layer spacing of ≈0.35 nm of graphene can be observed.

PEMG is ≈0.35 nm, consistent with the result of X-ray diffraction (XRD) (Figure 2f and Figure S5, Supporting Information).

In order to characterize the effect of the wrapped graphene on the reaction system, high-frequency structure simulator (HFSS) has also been used to simulate the electric field distribution in the reaction chamber. It can be found that the electric field intensity in the quartz tube passing through the reactor is the largest when there is no graphene coating (Figure 3b). This is advantageous for the preparation of high-quality graphene, but as the reaction progressed, the inner wall of the quartz tube in the reactor was gradually surrounded by graphene. The normalized electric field strength in the center of the quartz tube had drastically reduced ≈34% when the thickness of the wrapped graphene reached 50 μm (Figure 3c). At this time, it can be seen that the quality factor is continuously decreasing, and the proportion of energy loss is also increasing (Figure 3a), which is not conducive to continuous “snowing” graphene. Hence, it is necessary to “recover” the system for scalable production of PEMG. When employing PEMIS process, it is useful for continuous production of graphene without affecting the quality. Raman is used to quickly and non-destructively characterize the quality of graphene.^[26] It can be seen that PEMG possesses extremely high quality (Figure 3d, red line). The intensity ratio of I_D/I_G is as low as 0.3 or less (about 0.27), while the intensity ratio of I_{2D}/I_G is as high as 1 or more (about 1.06). The similar results are acquired of graphene obtained batch-to-batch without the assistance of “pulse-etching” tech-

nology. As shown in the black line of Figure 3d, the intensity ratio of I_D/I_G and I_{2D}/I_G is ≈0.28 and ≈1.15, respectively, indicating no obvious quality change of PEMG. By changing the microwave power and the concentration of carbon sources within a certain range, PEMG still maintains the characteristics of high quality, and PEMG shows good consistency (Figure S6, Supporting Information). X-ray photoelectron spectroscopy (XPS) reveals a decrease of element ratio of C/O of PEMG from ≈294 to ≈165 by the PEMIS process (Figure 3e). Further characterization proved that this was mainly because of the presence of adsorbed oxygen after the introduction of oxygen-containing etchant (Figure S8, Supporting Information), but should be mentioned that the oxygen content of the obtained PEMG is still as low as ≈0.6%. Moreover, the XPS survey in Figure 3e also shows that no heterogeneous elements have been introduced in graphene, revealing the high purity of graphene. In addition, thermogravimetric (TG) was conducted to characterize the purity of PEMG obtained (Figure 2f). A single oxidation peak as high as 755 °C in the corresponding derivative thermogravimetry (DTG) was found to confirm the highly crystalline feature of PEMG, and weight loss suggests that PEMG has almost no impurities. Compared with graphene obtained in a batch-to-batch manner, the TG curve remains almost the same. All these characteristics show that the PEMIS process can be applied to obtaining high-quality, low-oxygen content and high-purity PEMG powder, which is of great significance for large-scale preparation of graphene.

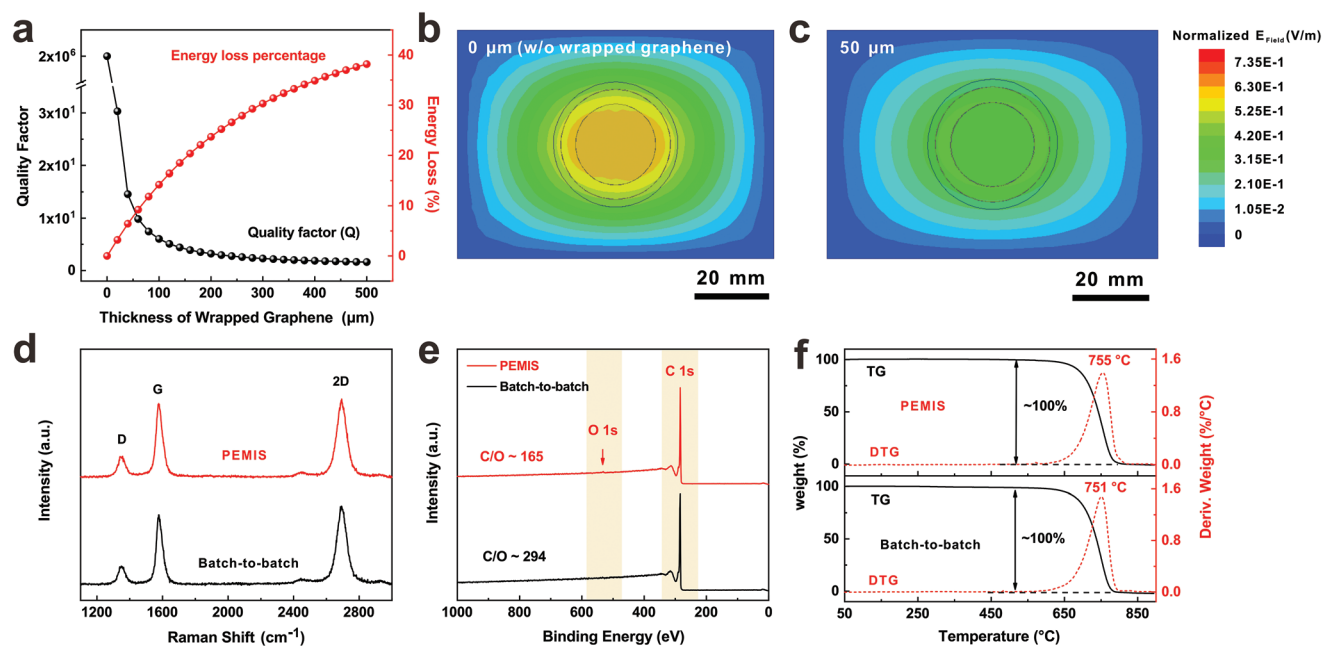


Figure 3. Effect of “pulse-etching” technology on PEMG. a) Plot of quality factor and energy loss versus the thickness of wrapped graphene. b,c) Simulation of electric field distribution in the reaction chamber with a wrapped graphene thickness of 0 and 50 μm by HFSS, respectively. The normalized electric field strength in the center of the quartz tube with a graphene thickness of 50 μm had drastically reduced ≈34% compared with that of empty one. d) Raman spectra, e) XPS and f) TG curves of PEMG by PEMIS process (with “pulse-etching” technology) or graphene from batch-to-batch production (w/o “pulse-etching” technology), indicating that the PEMIS process can be applied to continuous obtaining high-quality, low-oxygen content, and high-purity PEMG.

Similar to previous work,^[14] we also used in situ optical emission spectrum (OES) to monitor the reaction system, and can still find the peaks of CH, C₂, and Ar radicals (Figure S8, Supporting Information), further demonstrating that the carbon source is still fully cracked.

PEMG also shows microwave responsiveness at low frequency ignored by most.^[27] As can be seen in Figure S9, Supporting Information, the calculated reflection loss values of PEMG under frequency range from 0.1–3.0 GHz shows the microwave absorption properties of PEMG, and further analysis indicated that the main loss type of PEMG was dielectric loss (Figure S10, Supporting Information). Therefore, microwave can be absorbed by PEMG and then transformed to heat by dielectric loss or eddy current loss, making it possible for microwave heating. Taking consideration of the high quality and small size as well as microwave responsiveness of biocompatible PEMG, we explored its application in the field of MTT for tumors for the first time. At present, MTT, as an emerging tumor treatment method, has gained great attention on account of its longer penetration depth, short treatment time, and simple operation,^[22,28] but still requires satisfactory materials with proper size, and especially good microwave responsiveness as well as high thermal transformation efficiency at low frequency (below 2.45 GHz).^[29] Current MTT sensitization materials are mainly based on the principle of ions vibrating in a confined space,^[21,22] where there is a possibility of ion leakage resulting in unstable microwave heating performance and may also bring about potential toxicity. Therefore, PEMG could become an ideal material for MTT.

Figure 4a is a schematic diagram of PEMG-based MTT. PEMG was first noncovalently functionalized with a PEGylated phospholipid (DSPE-PEG₂₀₀₀),^[30] leading to easy dispersibility in saline solution. Then, 1-tetradecanol (PCM) was introduced to control the release of liposoluble drugs (Apatinib) to prepare the nanocomposites (DPA@PEMG). When stimulated by microwave, PEMG can absorb microwave for heat generation to promote thermal therapy. At the same time, the increase in temperature will contribute to the melting of PCM under microwave irradiation and then promote the release of drugs to achieve the purpose of in situ chemotherapy. In this way, combined in situ thermal therapy with chemotherapy for tumor treatment in vivo can be achieved.

By monitoring the temperature rise of the microwave heating effect in vitro with FLIR system, it was found that a microwave irradiation of 450 MHz and 1.8 W for 5 min can increase the temperature of pure saline solution by 16.6 °C, while the heating effect of non-covalently functionalized PEMG becomes more significant as the concentration of PEMG increases. When the concentration of PEMG reaches 10 mg mL⁻¹, the temperature can be increased by 24.8 °C at the same condition (Figure 4b and Figure S11, Supporting Information), following a temperature rise of 8.2 °C in contrast with saline solution, which can further prove the good microwave absorption performance of PEMG. Considering the features of large surface area and no obvious functional groups of PEMG, it can be used as an ideal carrier for liposoluble drugs. PCM will undergo solid-liquid transition when increasing temperature to 38–40 °C. Therefore, under microwave irradiation, the PCM can act as a temperature-controlled switch to promote the further release of

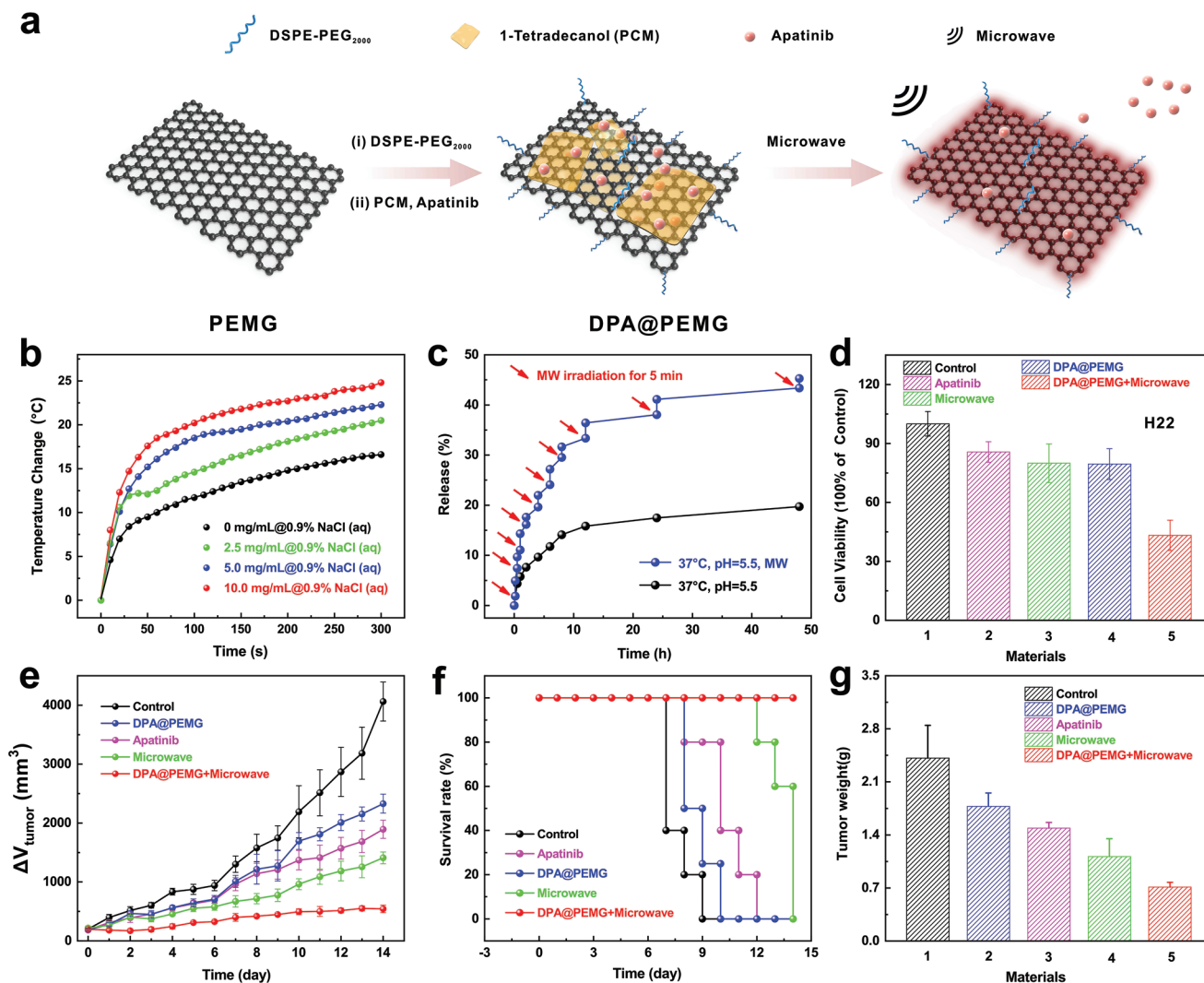


Figure 4. Performance of PEMG-based enhanced MTT. a) Schematic diagram of PEMG-based MTT. b) Temperature-rising effect of PEMG with different concentrations under a microwave irradiation of 450 MHz and 1.8 W for 5 min. c) Apatinib release rate of DPA@PEMG in different conditions. d) Cell viability of H22 cells treated in different conditions. e, f) Curves of tumor volume (e) and survival rate (f) of BALB/c mice during 14 days' treatment in different conditions. g) Tumor weight of mice on the 14th day treatment in different conditions.

Apatinib as can be seen in Figure 4c. The Apatinib release rate of DPA@PEMG is 19.71% at 37 °C, while that of DPA@PEMG can quickly increase to 45.29% when stimulated by microwave at the same conditions. The improved drug release rate of up to 25.58% can be ascribed to the perfect preparation of DPA@PEMG, providing the basis for the combination of MTT and chemotherapy for tumor treatment. It should be mentioned that the loading capacity of Apatinib is 22.18%. Under microwave irradiation, the temperature of the system was raised to approximately 45 °C. The drug release rate was 45.87% when performing DPA@PEMG directly at 45 °C, close to the drug release rate stimulated by microwave (Figure S12, Supporting Information), proving the temperature-controlled switch characteristics of PCM.

Mouse normal fibroblasts L929 and mouse hepatoma cells H22 were used to verify the cytotoxicity of DPA@PEMG, and showed that the DPA@PEMG was of very low cytotoxicity in cells (Figure S13, Supporting Information). Therefore, it can be

used in anti-tumor experiments in vitro and in vivo. After that, H22 cells were further used to evaluate the inhibitory effect of DPA@PEMG in vitro. When H22 cells were treated under control, Apatinib, microwave, DPA@PEMG, and DPA@PEMG + microwave in the same way, the final treatment reaches the lowest cell viability (Figure 4d). Only 43.24% of H22 cells survived, showing its excellent killing performance of tumor cells. It also showed that DPA@PEMG had excellent effects of thermal therapy and chemotherapy, which verified the previous assumptions.

The treatment effects of DPA@PEMG were further evaluated by BALB/c mice in vivo. DPA@PEMG was injected into the tail vein of BALB/c mice bearing H22 cancer cells for anti-tumor experiments in vivo. In the experiment, 6 h after injecting DPA@PEMG, we performed MTT experiments, while using FTIR system for temperature monitoring. The temperature of tumor tissue treated by injection of DPA@PEMG and then exposed in microwave irradiation can increase by nearly

17.8 °C, from 35.3 to 53.1 °C, while 12.5 °C of temperature increase can be reached only by that irradiated in microwave (Figures S14 and S15, Supporting Information). The increase of 5.3 °C can be attributed to the conversion of microwave to heat of DPA@PEMG, and the local heating contributes to local thermal therapy of this material for tumor ablation. It can be seen that no obvious body weight loss appeared in mice, indicating the good biocompatibility of DPA@PEMG (Figure S16, Supporting Information). The volume change of tumor tissue is presented in Figure 4e. A high tumor ablation rate of ≈86.7% can be achieved, showing the significant effect of MTT combined with chemotherapy of DPA@PEMG in vivo. In this work, we defined that it is equivalent to death of mice when tumor volume exceeded 1300 mm³. Therefore, the survival rate curve shown in Figure 4f demonstrated that the group of mice treated by DPA@PEMG with microwave exhibited a significantly higher survival rate (100%) than other groups. Photographs and weight of tumor are present in Figure S17, Supporting Information, and Figure 4g. It should be mentioned that one mouse in the group treated just with DPA@PEMG was dead of unknown causes on the 3rd day, therefore, the corresponding tumor tissue was missing. We can know that the tumor tissues in the experimental group (treated by DPA@PEMG + microwave) show the lightest weight and smallest volume, further validating the excellent effect of the combination of MTT and chemotherapy.

Besides taking advantage of the high quality and few layers of PEMG, leading to greatly intrinsic mechanical property maintenance, it can also be used as a high-performance reinforcement filler.^[31,32] It should be noted that the conventional preparation methods for graphene-based polymer composites usually concentrate on a solution-based method, which will bring about a lot of pollution and a complicated process.^[33,34] Usually, graphene oxide or reduced graphene oxide are primary choices, but the mechanical properties are poor, and graphene tend to agglomerate in the liquid phase system.^[35,36] In order to avoid these problems, we choose high-density polyethylene (HDPE) as a model system to demonstrate our strategy. A low mass fraction of original PEMG powder (1%), which means graphene collected directly in the gas phase, and HDPE are extruded after melt blending to obtain the PEMG@HDPE nanocomposites (Figure S18, Supporting Information). The Young's modulus of PEMG@HDPE can be improved by an average increase of ≈22.7% and a maximum increase of ≈29.6% compared to pure HDPE, while the average improvement of flexural modulus is ≈43.3% and ≈47.5% as maximum, showing good mechanical enhancement of PEMG (Figure S19, Supporting Information). The promotion of the mechanical properties can be contributed to the particularly uniform dispersion of PEMG in HDPE (Figure S20, Supporting Information). In situ TEM further confirms that the interfaces between graphene and HDPE are tightly bound (Video S1, Supporting Information).

In this work, we presented a PEMIS process for continuous and scalable preparation of graphene with high quality and high purity, which was found to have excellent thermotherapeutic effects. Typically, a high yield of ≈10.46% with high quality (I_D/I_G as low as ≈0.27 and I_{2D}/I_D as high as ≈1.06), high element ratio of C/O of ≈165, and high purity ≈100% of graphene can be obtained directly in the gas phase without substrate or

catalyst (Table S1, Supporting Information). It is demonstrated as graphene-based combination therapeutic system by virtue of the intrinsic characteristics of this small-sized (≈180 nm) biocompatible graphene, especially low-frequency microwave absorption property as well as good thermal transformation ability, for MTT for the first time, exhibiting a high tumor ablation rate of ≈86.7%. Besides, it exhibits a uniform dispersion of the graphene in polymer matrix in a very simple manner with significantly enhanced mechanical properties, demonstrating this graphene as a promising reinforcement filler. It is foreseen that this graphene can play multifunctional roles in various applications based on the associated intrinsic characteristics.

Experimental Section

Continuous "Snowing" Graphene via PEMIS Process: A surface wave type of plasma was created in the center of a quartz tube with internal diameter of 22 mm. The maximum power of microwave (2.45 GHz) provided by a generator (Sairem) was 2 kW. Argon (800–5000 cm³(STP) min⁻¹) was introduced into the tube to expel the residual air and then initiate the plasma at ambient pressure. A nominal amount of methane (2–20 cm³(STP) min⁻¹) was brought into the system for graphene preparation in the gas phase. After 20–30 min reaction, the inner wall of the tube was partially covered with black graphene. Then, replaced methane with oxygen (5–10 cm³ (STP) min⁻¹) to etch the wrapped graphene for 1–5 min, alternating methane and oxygen for continuous "snowing" graphene. Graphene powder could be obtained in the downstream or on the tube wall.

Preparation of DPA@PEMG: PEMG powder (10 mg) was dispersed in dichloromethane with DSPE-PEG₂₀₀₀. After evaporating the solvent, non-covalently functionalized PEMG could be obtained. Then, the obtained functionalized PEMG was mixed with Apatinib (11.4 mg), 1-tetradecanol (PCM, 12.9 mg), and absolute ethanol (2 mL). After it was well dispersed by ultrasonic dispersion, the mixed solution was under vacuum evaporation following washing the precipitate with anhydrous ethanol for three times and centrifuging (12 000 r min⁻¹) to obtain DPA@PEMG and collecting the three washing solutions for obtaining drug loading capacity by ultraviolet test.

In Vitro Cell Viability by DPA@PEMG: The H22 cells were cultured for 24 h in a six-well plate before use. Five groups of 1) control group: without any treatment, 2) Apatinib group: treated by free Apatinib, 3) microwave group: treated by microwave, 4) DPA@PEMG group: treated by DPA@PEMG, and 5) DPA@PEMG+Microwave group: treated by DPA@PEMG and microwave, were divided. The parameters of microwave were 450 MHz, 1.8 W, and 5 min. The concentration of DPA@PEMG was 50 μg mL⁻¹, and the content of Apatinib was kept the same in the above groups. After microwave irradiation, the H22 cells were transferred to 96-well plates for 24 h, following cell viability detection by methyl thiazolyl tetrazolium assay.

Animal Model: BALB/c mice were obtained from Beijing Vital River Laboratory Animal Technology Co., Ltd. and used according to the procedures approved by the experimental animal center of the Technical Institute of Physics and Chemistry, Chinese Academy of Sciences. H22 tumor was produced by injecting 1 × 10⁶ cells suspended in ≈150 μL PBS medium into the abdominal subcutaneous of each female BALB/c mouse. When the tumor volume reached about 200 ± 20 mm³, the anti-tumor experiments in vivo were performed.

In Vivo Tumor Inhibition by DPA@PEMG: Female BALB/c mice (22.5 ± 1 g) were randomly divided into the same five groups (five mice per group with a tumor volume of 200 ± 20 mm³) as mentioned above. After injection into the tail vein of mice with materials for 6 h, FLIR system was conducted to monitor the temperature and record the thermal images. Tumor volumes were calculated by the following equation: Tumor volumes = $a^2b/2$, where a is defined as the width and b is the length of the tumor. Tumor volume and weight of each mouse

were recorded daily. After 14 days, the mice were sacrificed for further study.

Characterization: TEM (FEI Tecnai F30; 300 kV) and aberration-corrected atomic-resolved TEM (Titan Cubed Themis G2 300; 80 kV) were conducted to investigate the morphology and structure of PEMG. Raman spectroscopy (Horiba Jobin Yvon LabRAM HR 800, 514.5 nm), XPS (Kratos Analytical Axis-Ultra spectrometer with Al K α X-ray source), XRD (D8 ADVANCE; Cu K α), and TG (Q600 SDT) were used to evaluate the quality, oxygen content, or impurity content of PEMG. SSA of PEMG was obtained by nitrogen adsorption–desorption isotherms of BET (MicrotracBEL BELSORP-max). The detection of radicals in the system was conducted by in situ OES (AvaSpec-ULS2048). For dielectric and magnetic spectra measurements, PEMG was mixed with paraffin (weight ratio of PEMG to paraffin is 1:2) to prepare toroidal shape samples, and then was analyzed by a vector network analyzer (PNA E8363B) from 0.1 to 3.0 GHz at room temperature.

Supporting Information

Supporting Information is available from the Wiley Online Library or from the author.

Acknowledgements

Y.S. and Z.C. contributed equally to this work. The authors specially thank Prof. Ciyuan Gao and Mr. Xinyong Duan at the University of Electronic Science and Technology of China for simulating the electric field distribution in the reaction chamber. The authors thank Prof. Jinbo Yang, Dr. Guanyi Qiao, and Mr. Yuankang Wang from Peking University for acquiring magnetic and dielectric spectra of PEMG. The authors thank Prof. Jingmin Zhang from Peking University for data collection of aberration-corrected atomic-resolved TEM images and EELS of PEMG. The authors also thank Prof. Yi Cheng from Tsinghua University for providing instrument of in situ OES. This research was supported by the Ministry of Science and Technology of China (2016YFA0200101) and the National Natural Science Foundation of China (Grant Nos. 51720105003, 21790052, 91859201, and 51972005).

Conflict of Interest

The authors declare no conflict of interest.

Keywords

graphene, microwave thermal therapy, scalable production

Received: March 24, 2020

Revised: April 7, 2020

Published online:

[1] C. Lee, X. D. Wei, J. W. Kysar, J. Hone, *Science* **2008**, 321, 385.

[2] A. A. Balandin, S. Ghosh, W. Z. Bao, I. Calizo, D. Teweldebrhan, F. Miao, C. N. Lau, *Nano Lett.* **2008**, 8, 902.

- [3] K. S. Novoselov, A. K. Geim, S. V. Morozov, D. Jiang, Y. Zhang, S. V. Dubonos, I. V. Grigorieva, A. A. Firsov, *Science* **2004**, 306, 666.
- [4] A. K. Geim, K. S. Novoselov, *Nat. Mater.* **2007**, 6, 183.
- [5] Y. W. Zhu, S. Murali, W. W. Cai, X. S. Li, J. W. Suk, J. R. Potts, R. S. Ruoff, *Adv. Mater.* **2010**, 22, 3906.
- [6] A. Zurutuza, C. Marinelli, *Nat. Nanotechnol.* **2014**, 9, 730.
- [7] W. Kong, H. Kum, S. H. Bae, J. Shim, H. Kim, L. P. Kong, Y. Meng, K. J. Wang, C. Kim, J. Kim, *Nat. Nanotechnol.* **2019**, 14, 927.
- [8] W. C. Ren, H. M. Cheng, *Nat. Nanotechnol.* **2014**, 9, 726.
- [9] L. Lin, H. L. Peng, Z. F. Liu, *Nat. Mater.* **2019**, 18, 520.
- [10] W. S. Hummers, R. E. Offeman, *J. Am. Chem. Soc.* **1958**, 80, 1339.
- [11] S. Bae, H. Kim, Y. Lee, X. F. Xu, J. S. Park, Y. Zheng, J. Balakrishnan, T. Lei, H. R. Kim, Y. I. Song, Y. J. Kim, K. S. Kim, B. Ozyilmaz, J. H. Ahn, B. H. Hong, S. Iijima, *Nat. Nanotechnol.* **2010**, 5, 574.
- [12] Y. Ando, X. Zhao, M. Ohkohchi, *Carbon* **1997**, 35, 153.
- [13] A. Dato, V. Radmilovic, Z. Lee, J. Phillips, M. Frenklach, *Nano Lett.* **2008**, 8, 2012.
- [14] Y. Y. Sun, L. W. Yang, K. L. Xia, H. Z. Liu, D. Han, Y. Y. Zhang, J. Zhang, *Adv. Mater.* **2018**, 30, 8.
- [15] H. B. Zhang, T. F. Cao, Y. Cheng, *Carbon* **2015**, 86, 38.
- [16] K. S. Novoselov, V. I. Fal'ko, L. Colombo, P. R. Gellert, M. G. Schwab, K. Kim, *Nature* **2012**, 490, 192.
- [17] Q. Y. He, S. X. Wu, Z. Y. Yin, H. Zhang, *Chem. Sci.* **2012**, 3, 1764.
- [18] Z. Liu, J. T. Robinson, X. M. Sun, H. J. Dai, *J. Am. Chem. Soc.* **2008**, 130, 10876.
- [19] M. Pumera, *Energy Environ. Sci.* **2011**, 4, 668.
- [20] H. F. Song, J. M. Liu, B. L. Liu, J. Q. Wu, H. M. Cheng, F. Y. Kang, *Joule* **2018**, 2, 442.
- [21] L. F. Tan, W. T. Tang, T. L. Liu, X. L. Ren, C. H. Fu, B. Liu, J. Ren, X. W. Meng, *ACS Appl. Mater. Interfaces* **2016**, 8, 11237.
- [22] Z. Z. Chen, M. Niu, G. Chen, Q. Wu, L. F. Tan, C. H. Fu, X. L. Ren, H. S. Zhong, K. Xu, X. W. Meng, *ACS Nano* **2018**, 12, 12721.
- [23] M. Fronczak, P. Fazekas, Z. Karoly, B. Hamankiewicz, M. Bystrzejewski, *Chem. Eng. J.* **2017**, 322, 385.
- [24] C. Melero, R. Rincon, J. Munoz, G. Zhang, S. Sun, A. Perez, O. Royuela, C. Gonzalez-Gago, M. D. Calzada, *Plasma Phys. Controlled Fusion* **2018**, 60, 014009.
- [25] J. Toman, O. Jasek, M. Snirer, T. Kudrle, J. Jurmanova, *J. Phys. D: Appl. Phys.* **2019**, 52, 265205.
- [26] A. C. Ferrari, J. C. Meyer, V. Scardaci, C. Casiraghi, M. Lazzeri, F. Mauri, S. Piscanec, D. Jiang, K. S. Novoselov, S. Roth, A. K. Geim, *Phys. Rev. Lett.* **2006**, 97, 187401.
- [27] F. B. Meng, H. G. Wang, F. Huang, Y. F. Guo, Z. Y. Wang, D. Hui, Z. W. Zhou, *Compos. Part B* **2018**, 137, 260.
- [28] S. P. Wang, L. F. Tan, P. Liang, T. L. Liu, J. Z. Wang, C. H. Fu, J. Yu, J. P. Dou, L. Hong, X. W. Meng, *J. Mater. Chem. B* **2016**, 4, 2133.
- [29] H. T. Shi, T. L. Liu, C. H. Fu, L. L. Li, L. F. Tan, J. Z. Wang, X. L. Ren, J. Ren, J. X. Wang, X. W. Meng, *Biomaterials* **2015**, 44, 91.
- [30] L. Lin, L. Liu, B. Zhao, R. Xie, W. Lin, H. Li, Y. Y. Li, M. L. Shi, Y. G. Chen, T. A. Springer, X. Chen, *Nat. Nanotechnol.* **2015**, 10, 465.
- [31] J. N. Coleman, *Acc. Chem. Res.* **2013**, 46, 14.
- [32] J. J. Liang, Y. Huang, L. Zhang, Y. Wang, Y. F. Ma, T. Y. Guo, Y. S. Chen, *Adv. Funct. Mater.* **2009**, 19, 2297.
- [33] G. Goncalves, P. Marques, A. Barros-Timmons, I. Bdkin, M. K. Singh, N. Emami, J. Gracio, *J. Mater. Chem.* **2010**, 20, 9927.
- [34] W. S. Gao, Y. Lu, Y. Z. Chao, Y. Ma, B. C. Zhu, J. J. Jia, A. P. Huang, K. F. Xie, J. G. Li, Y. X. Bai, *J. Phys. Chem. C* **2017**, 121, 21685.
- [35] C. Gomez-Navarro, M. Burghard, K. Kern, *Nano Lett.* **2008**, 8, 2045.
- [36] M. K. Shukla, K. Sharma, *Polym. Sci., Ser. A* **2019**, 61, 439.